Solar Energy 178 (2019) 215–221

Contents lists available at ScienceDirect

Solar Energy

journal homepage: www.elsevier.com/locate/solener

Study of degradation in InGaP/InGaAs/Ge multi-junction solar cell characteristics due to irradiation-induced deep level traps using finite element analysis

Siva Kotamraju[a,*], M. Sukeerthi[a], Suresh E. Puthanveettil[b], M. Sankaran[b]

[a] IIIT Chittoor, Sri City, Andhra Pradesh 517646, India
[b] U.R. Rao Satellite Centre, Bengaluru 560017, India

ARTICLE INFO

Keywords:
III-V multi-junction solar cell
Trap level
Minority electron lifetime
Device modeling

ABSTRACT

We investigated the influence of irradiation-induced deep level traps on the performance of 3J solar cell using two-dimensional numerical simulations. Modeling of solar cell degradation has been performed by systematically considering the trap levels in the top InGaP and middle InGaAs subcells. At the trap concentration of $1 \times 10^{16}\,cm^{-3}$, simulation results show a conversion efficiency of 26% for AM0 spectrum (1-sun). The results obtained demonstrate that the trap level in p-base InGaAs causes more degradation compared to p-base InGaP region. The combination of $1 \times 10^{16}\,cm^{-3}$ trap concentration and $1 \times 10^{4}\,cm\,s^{-1}$ surface recombination velocity is the point beyond which significant reduction in solar cell output parameters was observed. For the same trap concentration and interface recombination values, 30% conversion efficiency was achieved at concentrated sunlight with current matching among the top and middle cells.

1. Introduction

Solar cells designed and developed using III-V semiconductor materials are specifically used for space photovoltaic conversion application due to lightweight and high efficiency compared to Si cells (Liou and Wong, 1992; Razykov et al., 2011). The combination of InGaP/GaAs on Ge substrate was extensively explored for space applications (Stan et al., 2008; Takamoto et al., 2014) and are currently being used in commercial satellites (Fetzer et al., 2007; Yoon et al., 2005). GaAs and Ge layers are lattice mismatched by 0.08% that causes internal thermal stress among the layers. This degrades the overall cell performance by generating misfit dislocations in GaAs layers. To lattice match all the layers, InGaAs middle cell is considered by adding 1% indium to GaAs (Rabady and Manasreh, 2017; Yamaguchi et al., 2005). This results in excellent lattice matching among all the layers and absorption covering wavelengths from 230 nm to 1900 nm (Meusel et al., 2003). Till date, efficiencies in the range of 31–46% were reported under 1 sun AM0 spectrum (Zhang et al., 2017) and concentrated sunlight using AM1.5 spectrum (Green et al., 2018). Minority carrier lifetime in the base layer plays a crucial role in defining the parameters of the solar cell. Deep level traps acting as recombination centers could be one of the primary reasons responsible for lifetime degradation. Apart from some native traps, InGaP and InGaAs layers are almost dislocation free layers when grown on lattice matched Ge substrate. Also, these layers contain low concentrations of native recombination centers having negligible influence on the short circuit current density. However, in space environment, these subcells are usually subjected to multiple energetic particles such as electrons and protons. By considering particles of one kind, a reasonable assessment of degradation in solar cell parameters can be made (Wang and Wang, 2014). The irradiation due to electrons usually results in the introduction of deep level traps within the bandgap. The trap concentration is referred by the following relation $N_t = k\phi$, where k is the introduction rate of non-radiative recombination centers in cm^{-1} and ϕ is the irradiation fluence in electrons cm^{-2}. At 1 MeV electron irradiation, depending on the fluence in the range of 1×10^{14}–1×10^{16} electrons cm^{-2}, multiple trap levels have been reported in GaAs and InGaP (Khan et al., 2000; Mazouz et al., 2013; Stievenard et al., 1986). It has been experimentally verified in case of GaAs that one electron trap (E_c–0.9) degrades the solar cell performance (Danilchenko et al., 2008; Stievenard et al., 1986). Modeling of individual subcell and the total cell was reported earlier in (Makham et al., 2010; Walters et al., 2011). However, there was no attempt to model the complete 3J solar cell by taking all the specific degradation causing deep level traps due to electron irradiation into account. The novelty of this paper lies in quantitatively assessing the total and individual cell degradation with respect to trap concentration

* Corresponding author.
E-mail addresses: siva.k@iiits.in (S. Kotamraju), sukeerthi.m@iiits.in (M. Sukeerthi), eps@isac.gov.in (S.E. Puthanveettil), msankar@isac.gov.in (M. Sankaran).

https://doi.org/10.1016/j.solener.2018.12.036
Received 8 October 2018; Received in revised form 24 November 2018; Accepted 15 December 2018
Available online 20 December 2018
0038-092X/

by selectively choosing the trap levels that are responsible for such degradation. While there has been reports on solar cell parameter variation with respect to fluence, there is no such study with respect to trap concentration. This is because of the concentration of recombination centers and their corresponding capture cross sections were not identified. We considered a wide range of trap concentration by identifying trap levels and their corresponding capture cross section.

The incident energetic particles such as electrons on solar cell tend to lose their energy upon impact by getting ionized. This results in displacing the atoms from its original position in the semiconductor lattice, eventually leading to point like defects (vacancies or interstitials) in the materials. Due to this phenomenon, energy levels are formed within the bandgap of the material acting as trapping or recombination centers. The trap distribution due to electron irradiation is uniformly distributed in the material (Bourgoin and De Angelis, 2001) and the same is taken into account in our simulations. In this paper, we present a model for InGaP and InGaAs that elucidates how the trap concentration influences diffusion length of minority carriers in the p-base layer at a specific capture cross section. Table 2 lists the details of the non-radiative recombination centers that are taken into account in this study. Increase in trap concentration (or fluence) results in reduced diffusion length, which in turn reduces J_{sc}, V_{oc}, impacting the conversion efficiency significantly. The device creation, J-V curve plotting and parameter extraction were performed using Apsys device simulator from Crosslight Inc., (APSYS, 2016). The software is based on 2D finite element analysis and is designed to model semiconductor devices by solving Poisson's equation and drift/diffusion equations for electrons and holes. Modeling of multi-junction solar cells using Crosslight APSYS was reported earlier in (Li et al., 2006, 2007). Modeling of multi-junction solar cells using other tools such as Silvaco Atlas (Michael, 2005) has also been reported. The data results have been validated with experimental results for 1 J and 3J solar cells using such tools. InGaP and InGaAs materials have been studied separately as single cells with respect to fluence (Bourgoin and De Angelis, 2001). The modeling and nature of defects in such materials have been studied in (Bourgoin and Zazoui, 2002; Gladney, 2004). As a subcell in a 3J solar cell, their degradation analysis has been analyzed and addressed with respect to trap concentration in this paper. All the simulation results reported in this paper are at 1-sun using AM0 spectrum (1346 W m^{-2}). Schematic illustration of 3J solar structure is shown in Fig. 1. Fig. 2 shows the J-V characteristics comparing the experimental structure and our simulated structure. Our structure was further optimized for better efficiency (η = 31.8%) and the optimized curve shown in dotted lines. Anti-reflective coating (ARC) consisting of MgF_2 and ZnS stack with thickness 90 nm and 52 nm respectively stacked on top of the solar cell were considered (Jiang Lin et al., 2013; Saylan et al., 2015). The ARC thickness values were increased to 110 nm and 62 nm to optimize the solar cell efficiency. The basic cell design principles such as thicker base than emitter, highly doped emitter than the base, n on p, etc., were taken into consideration. 3J solar cells generally are stacked in such a way that top subcell has the higher bandgap p-n junction (1.86 eV) and the bottom subcell with the lowest bandgap (0.67 eV). All the subcells are connected by the tunnel diodes forming a low resistance path for the current to flow. Highly doped AlGaAs tunnel junctions were considered between top-middle and middle-bottom subcells as it will yield better efficiency (Özen et al., 2015). Each subcell consists of four layers namely window, emitter, base and back surface field (BSF) layers. Window and BSF are wider bandgap materials compared to emitter and base, mainly used to suppress the interface recombination whilst allowing photons to pass through the emitter base p-n junction. Having an n-emitter and p-base (n on p) gives better efficiency values compared to n-base and p-emitter (p on n). This is because of p on n structures leads to a knee in the I-V curve reducing the fill factor and hence the efficiency of solar cell (Wang and Wang, 2014). In this paper, the effect of trap concentration on J_{sc}, V_{oc}, and efficiency is systematically studied for a three-junction InGaP/InGaAs/Ge solar cell structure. This is an

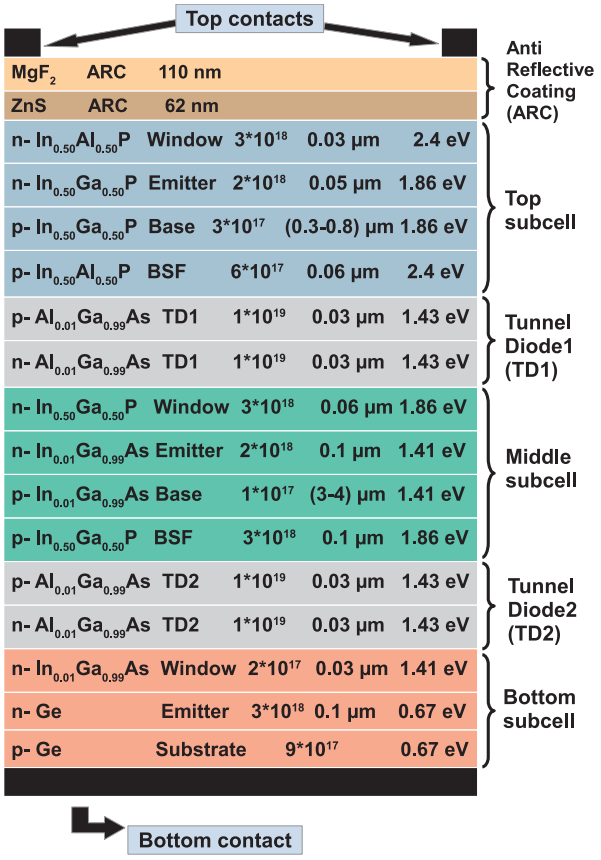

Fig. 1. Illustration of 3J InGaP/InGaAs/Ge solar cell (doping values in cm^{-3}).

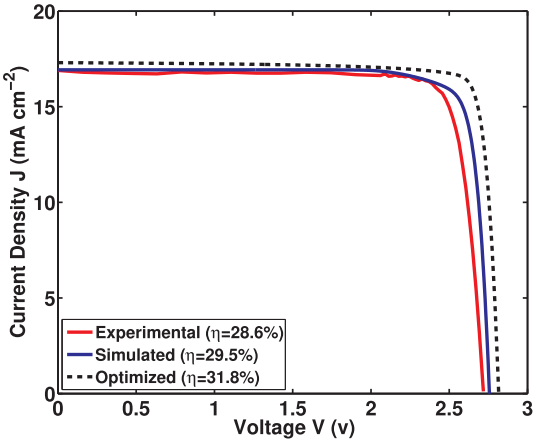

Fig. 2. 3J InGaP/InGaAs/Ge solar cell experimental and simulated current density vs. voltage characteristics (η stands for efficiency of 3J solar cell).

indirect assessment of solar cell degradation when subjected to irradiation in space. The importance of current matching with deep levels and interface recombination considerations to get the maximum efficiency is emphasized in our paper.

2. Simulation model

A model has been proposed taking the material parameters listed in Table 1 into consideration. This model relates minority carrier diffusion length with varying trap concentration in the base layer. The approximate values of capture cross section used in the model correspond to the trap levels that are defined in Table 2. Since lifetime in the thick base region is more critical than in the thin emitter region, minority

Table 1
Material parameters of InGaAs, InGaP.

Parameters (Symbol, Units)	InGaAs	InGaP
Bandgap (E_g, eV)	1.405	1.85
Effective mass (m_n)	0.067 (Raymond et al., 1979)	0.11 (Besikci and Razeghi, 1994)
Minority electron lifetime (τ_n^0, ns)	20 (Jain and Hudait, 2013)	5 (Tukiainen et al., 2014)
Mobility (μ_n, $cm^2 V^{-1} s^{-1}$)	3000 (Walukiewicz et al., 1979)	400 (Schultes et al., 2013)
Diffusion coefficient (D_n, $cm^2 s^{-1}$)	77.58	10.34

Table 2
Trap levels, trap type, and capture cross section values of InGaAs, InGaP.

Material	Trap level (eV)	Type	Capture cross section σ (cm^2)
InGaAs	$E_c - 0.9$	Acceptor	2×10^{-12} (Danilchenko et al., 2008)
InGaP	$E_c - 0.36$	Acceptor	3×10^{-17} (Khan et al., 2002)
	$E_c - 0.72$	Acceptor	2.5×10^{-17} (Khan et al., 2002)
	$E_v + 0.5$	Donor	4×10^{-16} (Khan et al., 2002)
	$E_v + 0.76$	Donor	5×10^{-16} (Khan et al., 2002)

carrier electrons in p-InGaAs and p-InGaP were considered in this model. This assumption was made based on the fact that irradiation-induced traps in the p-type base layer are the main traps causing degradation (Khan et al., 2000; Stievenard et al., 1986). The effective lifetime τ_n can be expressed as:

$$\frac{1}{\tau_n} = \frac{1}{\tau_n^0} + \frac{1}{\tau_{rad}} + \frac{1}{\tau_{nonrad}} \quad (1)$$

where τ_n^0 is minority electron lifetime without traps, τ_{rad} is the lifetime due to radiative recombination, and τ_{nonrad} is the lifetime due to non-radiative recombination. τ_{rad} usually has negligible influence on multi-junction solar cell characteristics and can be neglected. τ_{nonrad} is expressed as:

$$\tau_{nonrad} = \frac{1}{N_t \sigma v_{th}} \quad (2)$$

where N_t, σ are trap concentration in cm^{-3} and capture cross section in cm^2 respectively and v_{th} is thermal velocity in $cm\,s^{-1}$. v_{th} can be expressed as:

$$v_{th} = \sqrt{\frac{8kT}{\pi m_n}} \quad (3)$$

where k, T, and m_n are Boltzmann constant, temperature, and effective mass respectively. The value of m_n is taken from Table 1. The diffusion length L_n is given by:

$$L_n = \sqrt{D_n \tau_n} \quad (4)$$

where D_n is diffusion coefficient in $cm^2\ s^{-1}$ and is given by:

$$D_n = \frac{kT}{q}\mu_n \quad (5)$$

where μ_n is mobility in $cm^2 V^{-1} s^{-1}$. Our attempt was to accurately model solar cell degradation by sorting out those recombination centers with their corresponding capture cross section values that are non-radiative.

Several trap levels are usually created by irradiation. However, it was experimentally proven in (Khan et al., 2002) that $E_c - 0.36$, $E_c - 0.72$, $E_v + 0.5$, and $E_v + 0.76$ are the main non-radiative recombination centers for InGaP layers. Similarly, in (Danilchenko et al., 2008), it was demonstrated that $E_c - 0.9$ is responsible for degradation in GaAs. Instead of four different curves for InGaP, the diffusion length versus trap concentration was approximately modeled for two different capture cross sections $3 \times 10^{-17}\,cm^2$ and $4 \times 10^{-16}\,cm^2$ (Khan et al., 2002). Fig. 3a and b show the modeled diffusion length versus trap concentration for InGaAs and InGaP respectively. The experimental diffusion length versus trap concentration for p-InGaP and p-InGaAs is marked in Fig. 3a and b indicating a good agreement between the model and the experimental results (De Angelis et al., 2001; Gauffier et al., 2008; Khan et al., 2002). The experimental lifetime values reported in (De Angelis et al., 2001; Khan et al., 2002) are used for calculating diffusion length considering the capture cross section values listed in Table 2.

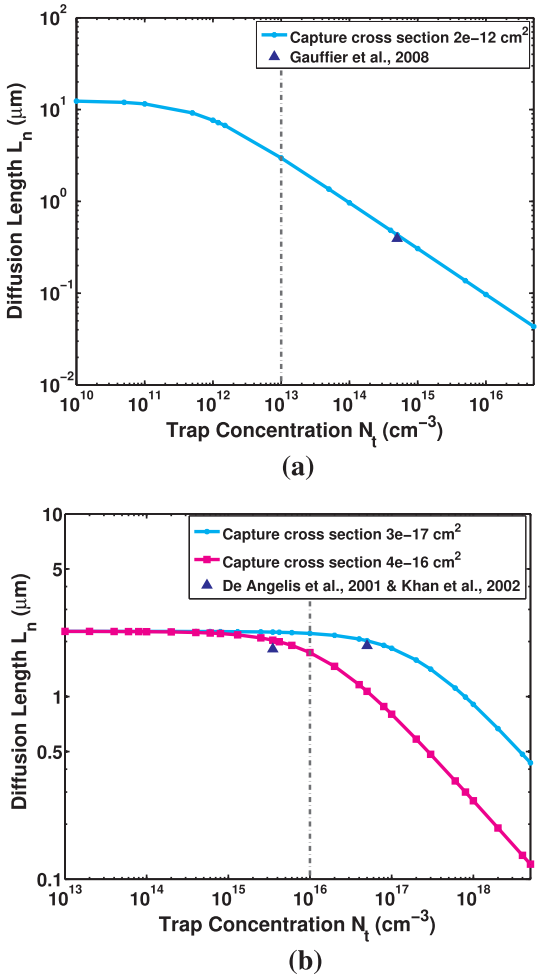

Fig. 3. Simulation model showing variation of diffusion length with increasing trap concentration for (a) InGaAs at a fixed capture cross section $2 \times 10^{-12}\,cm^2$. (b) InGaP at capture cross section values $3 \times 10^{-17}\,cm^2$ and $4 \times 10^{-16}\,cm^2$.

3. Results

This section is segregated into four subsections. In Section 3.1, trap analysis is done separately for top and middle cell. This will give an understanding of solar cell parameter degradation due to individual subcell traps. Following this, a combined trap analysis for both top and the middle cell are presented in Section 3.2. In Section 3.3, the influence of surface recombination velocity (SRV) of each subcell and complete cell on efficiency of solar cell is investigated. Finally, in Section 3.4, current mismatch and the optimization process for

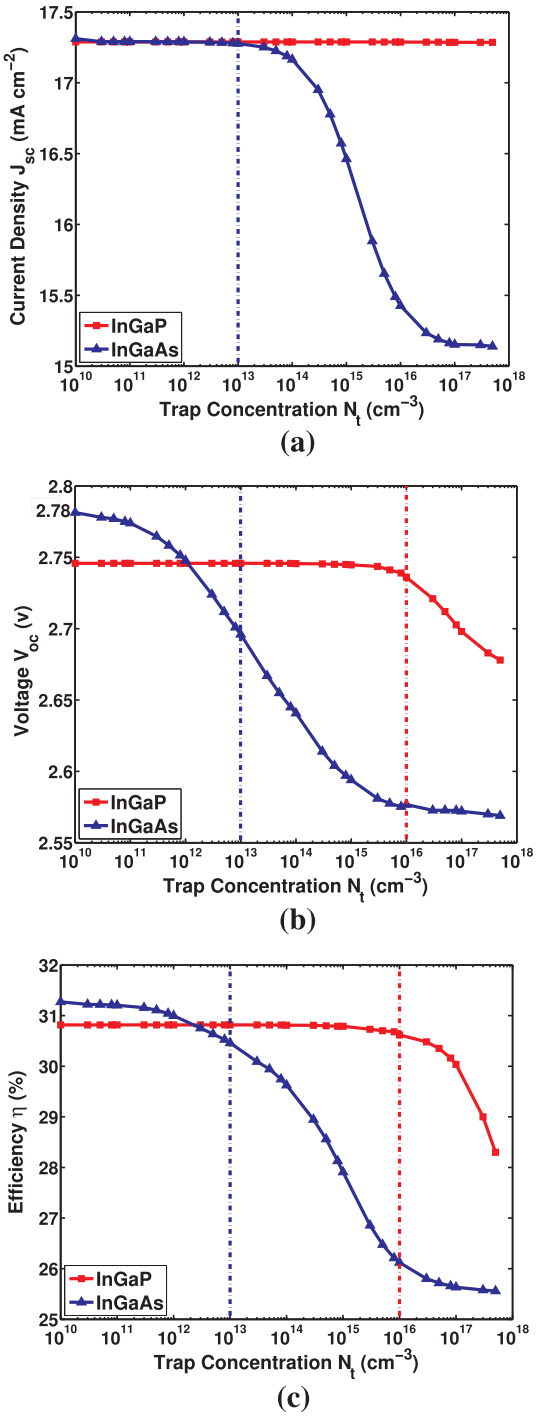

Fig. 4. Variation of (a) short circuit current density J_{sc} (b) open circuit voltage V_{oc} and (c) conversion efficiency η of 3J InGaP/InGaAs/Ge solar cell as a function of trap concentration with traps introduced in top InGaP cell (red line) and middle InGaAs cell (blue line) separately. (For interpretation of the references to color in this figure legend, the reader is referred to the web version of this article.)

obtaining a current matching for the top and middle cells are presented. Considering a realistic SRV and trap concentration values, P-V and EQE analysis is presented in Section 3.4. Initially, the thickness and doping of each subcell was chosen to get the highest efficiency possible. Before proceeding with the trap analysis, the base thickness of p-InGaAs and p-InGaP was fixed at 4 μm and 0.4 μm respectively. The overall efficiency of the solar cell was 31.8% (1-sun) with total Jsc value equal to 17.3 mA cm^{-2}. The SRV was fixed at 10^4 cm s^{-1} at the interface between emitter-window and base-BSF.

3.1. Separate trap analysis for the top and middle cell

On the assumption that irradiation influences only the top cell in a multi-junction solar cell structure, trap levels were defined within the bandgap of InGaP. Two majority and two minority level traps were defined in the base region with the capture cross section specified in Table 2. J_{sc}, V_{oc}, and η were plotted as a function of increasing trap concentration from 1×10^{13} cm^{-3} to 5×10^{17} cm^{-3} as shown in Fig. 4a, b, and c. For the trap concentration in the range of 1×10^{13} cm^{-3} to 1×10^{16} cm^{-3}, the efficiency was close to 31%. Beyond 1×10^{16} cm^{-3}, the efficiency started dropping and was 27.5% at 5×10^{17} cm^{-3} as shown in Fig. 4c. Higher J_{sc}, V_{oc} and η at a low trap concentration can be attributed to higher diffusion length in the p-InGaP base layer. For the trap concentration beyond 1×10^{17} cm^{-3}, diffusion length falls below the thickness of p-InGaP (0.4 μm) resulting in moderate degradation of J_{sc}, V_{oc} and η. Negligible drop in efficiency was observed for trap concentration below 1×10^{16} cm^{-3}. Interestingly, the percentage drop in J_{sc} is much less compared to V_{oc}, for the entire trap concentration investigated. At a realistic space condition of 1×10^{16} cm^{-2} 1 MeV electron irradiation, a total of 1×10^{16} cm^{-3} traps could be introduced in InGaAs and InGaP layers (Makham et al., 2010). At the trap concentration of 1×10^{16} cm^{-3} introduced only in InGaP, cell efficiency was observed to be 30%. Beyond 1×10^{16} cm^{-3}, cell efficiency moderately reduced due to diffusion length significantly becoming smaller than the thickness of the base region. To understand the influence of deep level traps in InGaP and InGaAs separately, trap levels are defined only in the middle InGaAs subcell. The blue line in Fig. 4a, b, and c correspond to the middle subcell. From Fig. 4a, it can be seen that J_{sc} is almost constant up to 1×10^{13} cm^{-3} trap concentration. Beyond that, J_{sc} of middle subcell starts reducing, while for the top subcell it is almost unaffected within the trap concentration investigated. Similar trend can be observed for V_{oc} in case of middle subcell. As expected, considering J_{sc} and V_{oc} trends, the efficiency also degrades drastically beyond 1×10^{13} cm^{-3} trap concentration for middle subcell. Clearly from Fig. 4, it can be concluded that middle subcell causes significant degradation in solar cell parameters compared to top cell.

3.2. Trap analysis for total solar cell

In this study, trap levels were introduced in both top and middle subcells with the capture cross section as specified in Table 2. The trap concentration in both top and middle subcells were varied simultaneously from 1×10^{10} cm^{-3} to 5×10^{17} cm^{-3}. J_{sc} and V_{oc} were plotted as a function of trap concentration, as shown in Fig. 5a and b. Fig. 5c shows the degradation of 3J InGaP/InGaAs/Ge solar cell efficiency η as a function of increasing trap concentration. Initially, the efficiency was 31% at trap concentration 1×10^{10} cm^{-3} and dropped to 24.6% at trap concentration 5×10^{17}cm^{-3}. With 1×10^{16} cm^{-3} taken as a reference point, the cell efficiency was about 25% compared to 30.6% and 26% in Fig. 4c. Unlike the InGaP efficiency trend shown in Fig. 4c, the onset of degradation in Fig. 5c started from much lower trap concentration (1×10^{13} cm^{-3}). The degradation in J_{sc}, V_{oc}, and η for trap concentration beyond 1×10^{13} cm^{-3} can be attributed to the simultaneous reduction of diffusion length in both p-InGaP and p-InGaAs. In other words, it is because of simultaneous recombination of photoexcited carriers in the p-regions of the top and middle cells. Even though it is one trap that is defined in p-InGaAs, the impact on solar cell parameters was found to be more significant. Reduction in diffusion length resulted in reduction of both J_{sc} and V_{oc}, thus reducing the cell efficiency significantly beyond 1×10^{16} cm^{-3}.

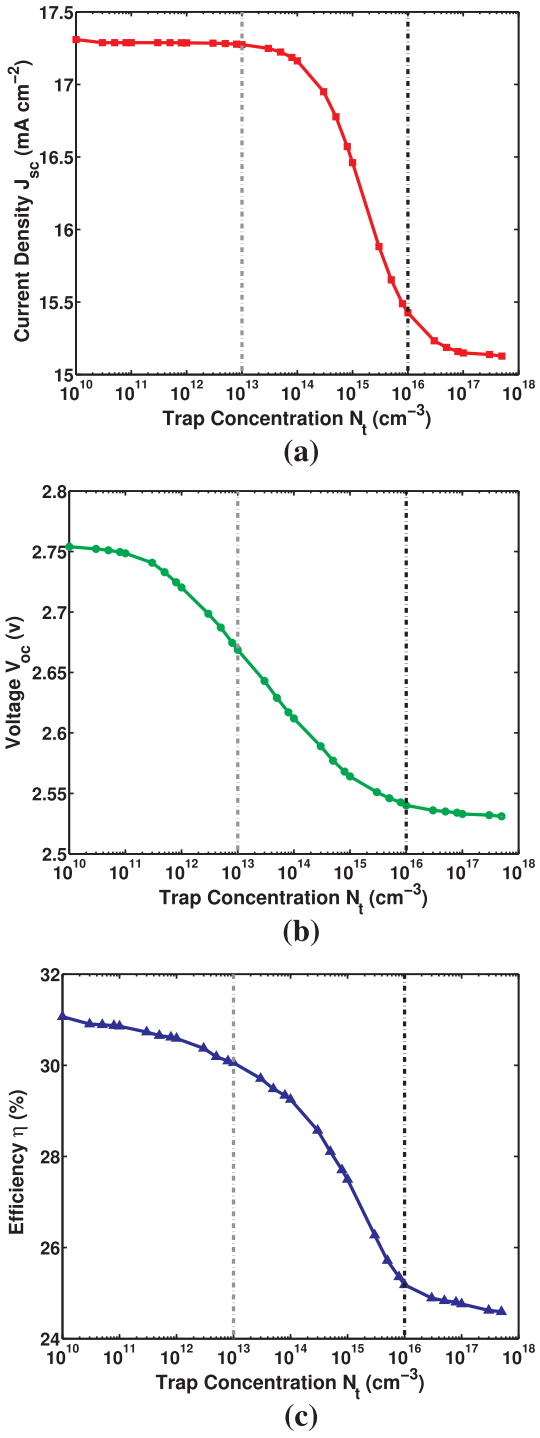

Fig. 5. 3J InGaP/InGaAs/Ge solar cell output parameter (a) J_{sc} (b) V_{oc} (c) η variation vs. trap concentration N_t with traps introduced in top InGaP and middle InGaAs cells simultaneously.

3.3. Interface recombination analysis

In the results discussed so far, an SRV of 10^4 cm s^{-1} was defined at all the emitter-window and base-back surface junctions for each subcell. It is interesting to see how the solar cell parameters would vary with respect to SRV at a fixed trap concentration of 1×10^{16} cm^{-3}. The SRV was fixed at 10^4 cm s^{-1} for InGaAs and Ge subcell and varied from 10^0 to 10^6 cm s^{-1} for InGaP top subcell to simulate the changes in η. Up to 10^4 cm s^{-1}, there seems to be no change in η, and beyond 10^4 cm s^{-1}, the efficiency starts dropping, although not considerably. The same

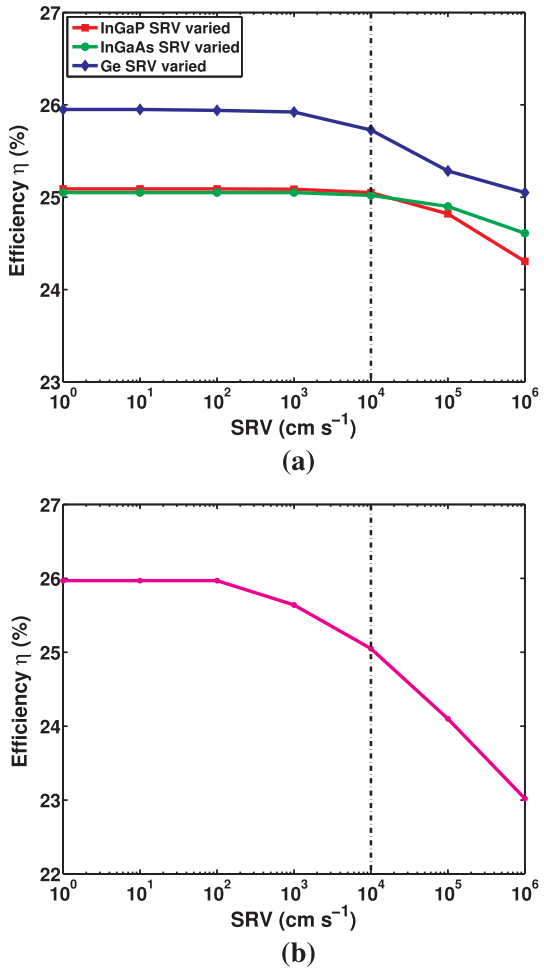

Fig. 6. Efficiency η as a function of SRV at trap concentration 1×10^{16} cm^{-3} with (a) SRV varied at top InGaP cell with SRV 10^4 cm s^{-1} at other junctions, SRV varied at middle InGaAs cell with SRV 10^4 cm s^{-1} at other junctions, SRV varied at bottom cell with SRV 10^4 cm s^{-1} at other junctions. (b) SRV varied at all cells simultaneously.

procedure is repeated for a fixed SRV of 10^4 cm s^{-1} for the top and middle subcells and varying at the bottom subcell as shown in Fig. 6a. The SRV at the bottom subcell seems to have minimum influence on the overall cell efficiency. Alternatively, in Fig. 6b, η is plotted by varying SRV at all the subcells simultaneously from 10^0 to 10^6 cm s^{-1}. Unlike trap concentration, it can be concluded that SRV has not significantly degraded η values even at 10^6 cm s^{-1}. On the other hand, restricting SRV to or below 10^4 cm s^{-1} can lead to optimum efficiency values.

3.4. Current matching

It is important to tailor the design of each subcell at a realistic trap concentration of 1×10^{16} cm^{-3} for closest current matching. After introducing SRV and traps, Fig. 7a shows the current mismatch among different subcells. As expected, due to lower bandgap, the bottom cell has the highest J_{sc} and lowest V_{oc}. Bottom subcell is therefore not the current limiting subcell. It can be observed that the middle cell is the current limiting subcell among all the three subcells. The next step is to make appropriate design changes especially to the top and middle subcell to realize current matching. Since the subcells are connected in series, it is known that the overall current is equal to the minimum current produced by the respective subcell. Fig. 7b shows the J-V curves of the solar cell after current matching. However, we could not get all the subcells exactly current matched with each other, but we tried to reach as close as possible. We obtained a minimum current density

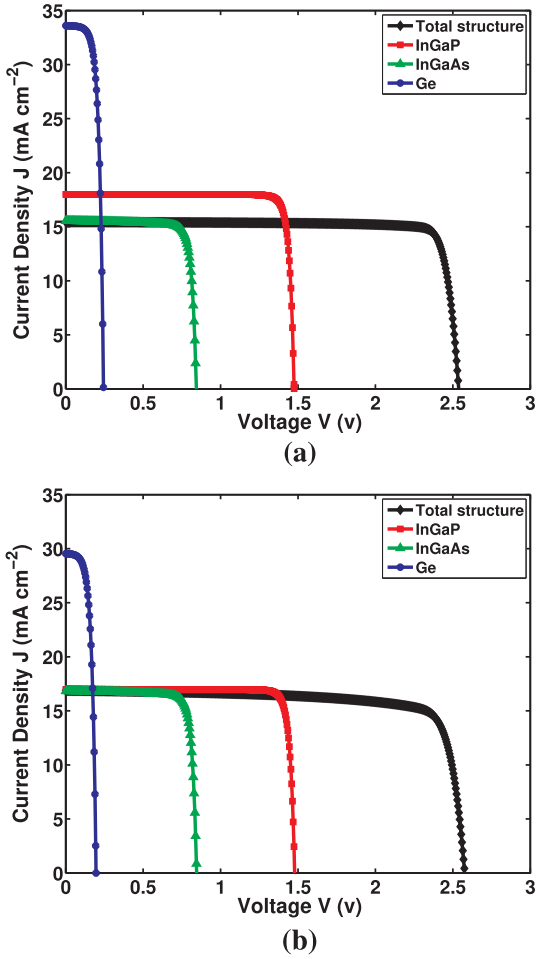

Fig. 7. Triple junction InGaP/InGaAs/Ge solar cell current density(J)-voltage (V) characteristics along with the InGaP, InGaAs and Ge subcells at trap concentration 1×10^{16} cm^{-3} and SRV 10^4 cm s^{-1} (a) current mismatched curves (b) current matched curves between top and middle subcell.

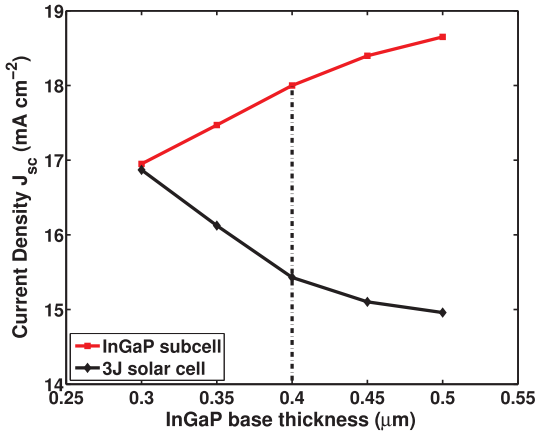

Fig. 8. Optimized thickness of top InGaP subcell for achieving current matching in 3J InGaP/InGaAs/Ge solar cell.

value equal to 16.87 mA cm^{-2}. A marginal increase in efficiency (from 25% to 26%) was observed after current matching. The thickness of the base region is the main parameter that was adjusted to get suitable current matching. Thickness optimization process to obtain current matching in the top cell is shown in Fig. 8. InGaP top cell base thickness was reduced from 0.4 μm to 0.3 μm to reduce the top subcell J_{sc} from 18 mA cm^{-2} to 17 mA cm^{-2}, while the total cell current density

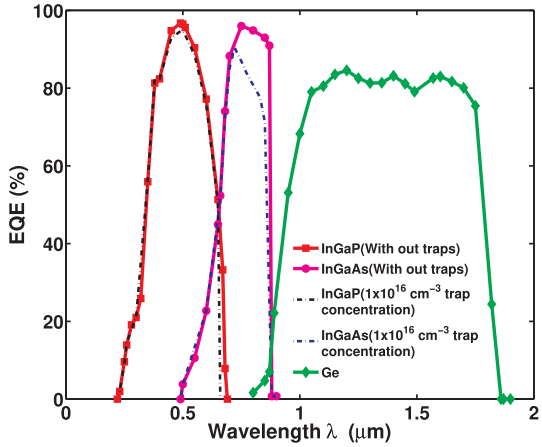

Fig. 9. Individual subcell spectral response of InGaP/InGaAs/Ge solar cell without defining traps (solid) and at trap concentration (dotted) 1×10^{16} cm^{-3} and SRV 10^4 cm s^{-1}.

increased from 15.4 mA cm^{-2} to 16.9 mA cm^{-2}.

The EQE curves of individual subcells are shown in Fig. 9. In the same figure, the individual spectral response with traps (dotted) is explicitly shown using AM0 spectrum. Without traps, the amplitude of EQE curves for the top and middle cells is above 90%, the amplitude of bottom cell is close to 80%. More degradation in the spectral response can be observed in the case of middle cell, which becomes the current limiting subcell after introducing traps. Taking into account the trap concentration of 1×10^{16} cm^{-3} and SRV of 10^4 cm s^{-1}, the sun concentration was varied from 1 to 500. It can be observed from Fig. 10 that peak efficiency of 30% was achieved at 200 suns and then the efficiency slowly started dropping. Variation in power density as a function of bias voltage is shown in Fig. 11. We calculated the power of each subcell and total structure with and without traps, based on the bias voltage of each subcell and the total structure. At a trap concentration of 1×10^{16} cm^{-3}, the drop in power density values is clearly seen. A peak power density of 35 mW cm^{-2} is obtained from the total structure with traps and SRV included. The drop in power density is more for middle cell compared to the top and bottom cells.

4. Conclusion

We have systematically studied the influence of specific deep level traps that are reportedly caused due to electron irradiation. The simulation model that is proposed appears to be consistent with the results obtained. The degradation of solar cell parameters with respect to trap

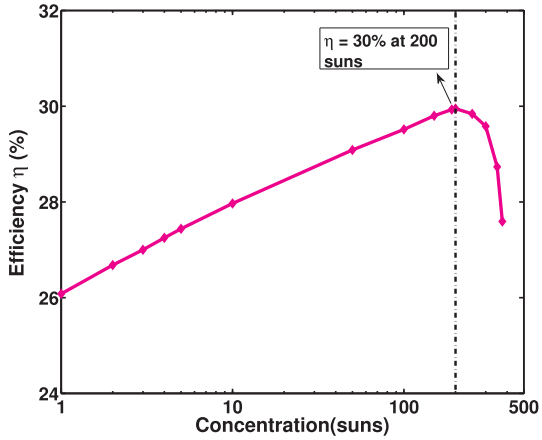

Fig. 10. Plot of efficiency versus sun concentration at 1×10^{16} cm^{-3} trap concentration and 10^4 cm s^{-1} SRV.

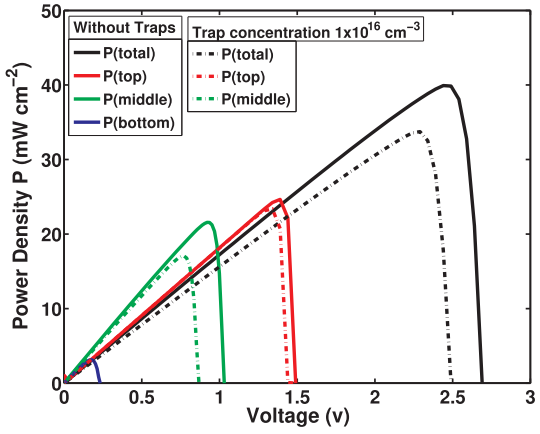

Fig. 11. P-V variation of total, top, middle, and bottom cells plotted without defining traps and by defining a trap concentration of $1 \times 10^{16}\,cm^{-3}$ and an SRV of $10^4\,cm\,s^{-1}$.

concentration appears to be qualitatively similar to the model proposed. The trap concentration considered from $1 \times 10^{10}\,cm^{-3}$ to $5 \times 10^{17}\,cm^{-3}$ should correspond to a wide range of irradiation fluence for a given introduction rate of non-radiative recombination centers. The results obtained illustrate that the recombination center in the middle cell is more responsible for degradation compared to the top cell. The variation in SRV from 10^0 to $10^6\,cm\,s^{-1}$ has a lesser impact on solar cell parameters compared to trap concentration. However, interface recombination in the top and middle subcells was found to have equal and more influence on efficiency compared to bottom subcell. Although not considerably, with deep levels taken into consideration, current matching does help in improving the overall efficiency of the solar cell. At a trap concentration of $1 \times 10^{16}\,cm^{-3}$ and an SRV of $10^4\,cm\,s^{-1}$ in top, middle and bottom cells, the 3J solar cell exhibited an efficiency of 30% under concentrated sunlight.

Acknowledgement

This work was supported by Indian Space Research Organization under Grant No. ISRO/RES/3/719/16-17. The authors would like to thank UR Rao satellite center for providing the experimental data of solar cell.

References

APSYS, 2016. Version by crosslight software inc., Burnaby, Canada, 2016.
Besikci, C., Razeghi, M., 1994. Electron transport properties of $Ga_{0.51}/In_{0.49}/P$ for device applications. IEEE Trans. Electron Dev. 41 (6), 1066–1069.
Bourgoin, J.C., De Angelis, N., 2001. Radiation-induced defects in solar cell materials. Sol. Energy Mater. Sol. Cells 66 (1–4), 467–477.
Bourgoin, J., Zazoui, M., 2002. Irradiation-induced degradation in solar cell: characterization of recombination centres. Semicond. Sci. Technol. 17 (5), 453.
Danilchenko, B., Budnyk, A., Shpinar, L., Poplavskyy, D., Zelensky, S.E., Barnham, K.W.J., Ekins-Daukes, N.J., 2008. 1MeV electron irradiation influence on GaAs solar cell performance. Sol. Energy Mater. Sol. Cells 92 (11), 1336–1340.
De Angelis, N., Bourgoin, J.C., Takamoto, T., Khan, A., Yamaguchi, M., 2001. Solar cell degradation by electron irradiation. Comparison between Si, GaAs and GaInP cells. Sol. Energy Mater. Sol. Cells 66 (1), 495–500.
Fetzer, C., King, R.R., Law, D.C., Edmondson, K.M., Isshiki, T., Haddad, M., Zhang, X., Boisvert, J.C., Joslin, D.E., Karam, N.H., 2007. Multijunction solar cell development and production at spectrolab.
Gauffier, A., David, J.P., Gilard, O., 2008. Analytical model for multi-junction solar cells prediction in space environment. Microelectron. Reliab. 48 (8), 1494–1499.
Gladney, D.C. 2004. Simulating radiation-induced defects on semiconductor devices. Technical report. Naval Postgraduate School, Monterey, CA.
Green, M.A., Hishikawa, Y., Dunlop, E.D., Levi, D.H., Hohl-Ebinger, J., Ho-Baillie, A.W.Y., 2018. Solar cell efficiency tables (version 52). Prog. Photovolt. Res. Appl. 26 (7), 427–436.
Jain, N., Hudait, M.K., 2013. Impact of threading dislocations on the design of GaAs and InGaP/GaAs solar cells on Si using finite element analysis. IEEE J. Photovolt. 3 (1), 528–534.
Jiang Lin, G., Bi, J., Song, M., Liu, J., Xiong, W., Huang, M., 2013. III-V multi-junction solar cells. In: Optoelectronics - Advanced Materials and Devices. InTech, Rijeka (Chapter 18).
Khan, A., Yamaguchi, M., Bourgoin, J.C., De Angelis, N., Takamoto, T., 2000. Room-temperature minority-carrier injection-enhanced recovery of radiation-induced defects in p-InGaP and solar cells. Appl. Phys. Lett. 76 (18), 2559–2561.
Khan, A., Yamaguchi, M., Bourgoin, J.C., Takamoto, T., 2002. Thermal annealing study of 1 MeV electron-irradiation-induced defects in n+ p InGaP diodes and solar cells. J. Appl. Phys. 91 (4), 2391–2397.
Li, Z.Q., Xiao, Y.G., Li, Z.S., 2006. Modeling of multi-junction solar cells by Crosslight APSYS. In: High and Low Concentration for Solar Electric Applications, vol. 6339. International Society for Optics and Photonics, pp. 633909.
Li, Z.Q., Xiao, Y.G., Li, Z.S., 2007. Two-dimensional simulation of GaInP/GaAs/Ge triple junction solar cell. Phys. Status Solidi C 4 (5), 1637–1640.
Liou, J.J., Wong, W.W., 1992. Comparison and optimization of the performance of Si and GaAs solar cells. Sol. Energy Mater. Sol. Cells 28 (1), 9–28.
Makham, S., Sun, G.C., Bourgoin, J.C., 2010. Modelling of solar cell degradation in space. Sol. Energy Mater. Sol. Cells 94 (6), 971–978.
Mazouz, H., Belghachi, A., Hadjaj, F., 2013. Solar cell degradation by electron irradiation effect of irradiation fluence. Simulation 14, 15.
Meusel, M., Baur, C., Létay, G., Bett, A.W., Warta, W., Fernandez, E., 2003. Spectral response measurements of monolithic GaInP/Ga (In) As/Ge triple-junction solar cells: Measurement artifacts and their explanation. Prog. Photovolt. Res. Appl. 11 (8), 499–514.
Michael, S., 2005. A novel approach for the modeling of advanced photovoltaic devices using the SILVACO/ATLAS virtual wafer fabrication tools. Sol. Energy Mater. Sol. Cells 87 (1–4), 771–784.
Özen, Y., Akın, N., Kınacı, B., Özçelik, S., 2015. Performance evaluation of a GaInP/GaAs solar cell structure with the integration of AlGaAs tunnel junction. Sol. Energy Mater. Sol. Cells 137, 1–5.
Rabady, R.I., Manasreh, H., 2017. Thicknesses optimization of two-and three-junction photovoltaic cells with matched currents and matched lattice constants. Sol. Energy 158, 20–27.
Raymond, A., Robert, J.L., Bernard, C., 1979. The electron effective mass in heavily doped GaAs. J. Phys. C: Solid State Phys. 12 (12), 2289.
Razykov, T.M., Ferekides, C.S., Morel, D., Stefanakos, E., Ullal, H.S., Upadhyaya, H.M., 2011. Solar photovoltaic electricity: current status and future prospects. Sol. Energy 85 (8), 1580–1608.
Saylan, S., Milakovich, T., Hadi, S.A., Nayfeh, A., Fitzgerald, E.A., Dahlem, M.S., 2015. Multilayer antireflection coating design for $GaAs_{0.69}P_{0.31}$/Si dual-junction solar cells. Sol. Energy 122, 76–86.
Schultes, F.J., Christian, T., Jones-Albertus, R., Pickett, E., Alberi, K., Fluegel, B., Liu, T., Misra, P., Sukiasyan, A., Yuen, H., Haegel, N.M., 2013. Temperature dependence of diffusion length, lifetime and minority electron mobility in GaInP. Appl. Phys. Lett. 103 (24), 242106.
Stan, M., Aiken, D., Cho, B., Cornfeld, A., Diaz, J., Korostyshevsky, A., Ley, V., Patel, P., Sharps, P., Varghese, T., 2008. Evolution of the high efficiency triple junction solar cell for space power. In: Photovoltaic Specialists Conference, 2008. PVSC'08. 33rd IEEE. IEEE, pp. 1–6.
Stievenard, D., Boddaert, X., Bourgoin, J.C., 1986. Irradiation-induced defects in p-type GaAs. Phys. Rev. B 34 (6), 4048.
Takamoto, T., Washio, H., Juso, H., 2014. Application of InGaP/GaAs/InGaAs triple junction solar cells to space use and concentrator photovoltaic. In: Photovoltaic Specialist Conference (PVSC), 2014 IEEE 40th. IEEE, pp. 0001–0005.
Tukiainen, A., Aho, A., Polojarvi, V., Guina, M., 2014. Modeling of MBE-grown GaInNAs solar cells. In: ESA Special Publication, vol. 719.
Walters, R.J., Messenger, S., Warner, J.H., Cress, C.D., Gonzalez, M., Maximenko, S., 2011. Modeling of radiation induced defects in space solar cells. In: Physics and Simulation of Optoelectronic Devices XIX, vol. 7933. International Society for Optics and Photonics, pp. 79330P.
Walukiewicz, W., Lagowski, J., Jastrzebski, L., Gatos, H.C., 1979. Minority-carrier mobility in p-type GaAs. J. Appl. Phys. 50 (7), 5040–5042.
Wang, X., Wang, Z.M., 2014. High-efficiency solar cells, Physics, materials, and devices. Springer Series in Materials Science, vol. 190.
Yamaguchi, M., Takamoto, T., Araki, K., Ekins-Daukes, N., 2005. Multi-junction III-V solar cells: current status and future potential. Sol. Energy 79 (1), 78–85.
Yoon, H., Granata, J.E., Hebert, P., King, R.R., Fetzer, C.M., Colter, P.C., Edmondson, K.M., Law, D., Kinsey, G.S., Krut, D.D., Ermer, J.H., 2005. Recent advances in high-efficiency III–V multi-junction solar cells for space applications: ultra triple junction qualification. Prog. Photovolt. Res. Appl. 13 (2), 133–139.
Zhang, L., Niu, P., Li, Y., Song, M., Zhang, J., Ning, P., Chen, P., 2017. Investigation on high-efficiency $Ga_{0.51}In_{0.49}P/In_{0.01}Ga_{0.99}As$/Ge triple-junction solar cells for space applications. AIP Adv. 7 (12), 125–217.